Tunneling characteristics and low-frequency noise of high-T_c superconductor/noble-metal junctions

Yizi Xu and J. W. Ekin
National Institute of Standards and Technology, Boulder, Colorado 80303, USA
(Received 20 December 2002; published 22 March 2004)

We report extensive measurements of transport characteristics and low-frequency resistance noise of *c*-axis yttrium-barium-copper-oxide (YBCO)/Au junctions. The dominant conduction mechanism is tunneling at low temperatures. The conductance characteristic is asymmetric, and the conductance minimum occurs at a nonzero voltage. These features can be qualitatively explained by modeling the YBCO/Au interface with a Schottky barrier. The model shows that the YBCO surface behaves like a *p*-type degenerate semiconductor, with a Fermi degeneracy of about 0.1 eV. The barrier height is approximately 1.0 eV. We present evidence that interface states and disorder play an important role in determining the conductance characteristics. Low-frequency noise measurements of these junctions reveal that junction noise is dominated by resistance fluctuations with a $1/f$-like power spectrum over a wide range of temperature and bias voltage. For temperatures between 4.2 and 77 K, the junction noise can be parameterized in terms of a normalized resistance fluctuation: $\delta R/R \simeq 6.3 \times 10^{-4}/\sqrt{f}$, in units of $\mathrm{Hz}^{-1/2}$, where f is the center frequency of the measurement bandwidth. At $f = 10$ Hz, for example, it is 2×10^{-4} $\mathrm{Hz}^{-1/2}$. This noise figure should prove to be useful for engineering design of high-T_c electronics. A more detailed analysis shows that at low temperatures the noise spectrum is characterized by random telegraph signals withe a Lorentzian power spectrum, which can have a distribution of corner frequencies that mimics a $1/f$ dependence. The random telegraph signals provide evidence for the existence of localized states.

DOI: 10.1103/PhysRevB.69.104515 PACS number(s): 74.72.Bk, 73.50.Td, 73.40.Gk

I. INTRODUCTION

High-temperature superconductor/noble-metal interfaces, such as the yttrium-barium-copper-oxide (YBCO)/Au interface, are an integral part of high-T_c electronic devices since they provide the basis for making wiring connections to the devices. In many cases, the electrical integrity of the interface plays an important role for the intended applications. For example, in the development of low-field magnetic resonance imaging (MRI) systems, YBCO thin films are used to make detection coils because they offer superior signal-to-noise ratio. It is thus very important that the contacts to the YBCO detection coils be both low resistance and low noise, so as not to compromise the benefits of using high-T_c materials. Therefore it is essential to understand the physical mechanisms of the interface conduction process. It is particularly important to measure and quantify the interface resistance noise, for which there are little systematic data.

In this paper, we report extensive measurements of transport characteristics of YBCO/Au junctions. We then present a simple interface-conduction model to account for these results, which suggests that localized states play an important role in determining the conduction characteristics. Finally, we present results of low-frequency noise measurements, from which we derive a noise figure that will prove to be valuable for engineering design. The noise measurement results also offer direct evidence for the influence of localized states.

II. JUNCTION FABRICATION

The YBCO thin films used in this work were prepared using pulsed laser deposition. The films were *c*-axis oriented, with T_c in the range of 87–91 K. We patterned our films using standard photolithography. One unique feature in our process is the use of an insulating layer of MgO to define small contact areas,[1] which varied from 2×2 $\mu\mathrm{m}^2$ to 16×16 $\mu\mathrm{m}^2$. The current flows nominally along the *c* axis of YBCO, through a native tunnel barrier, and into the Au electrode. The native tunnel barrier is formed on the surface of the *c*-axis-oriented YBCO film during the fabrication process, and is thought to consist of adsorbed impurities, as well as degraded topmost atomic layers of the YBCO film. The low-temperature resistance of our junctions ranged from a few Ω to a few hundred $\mathrm{k}\Omega$. The specific interface resistivity ρ_c, defined as the product of junction resistance and junction area, expressed in units of $\Omega\,\mathrm{cm}^2$, varies from a low of 10^{-4} $\Omega\,\mathrm{cm}^2$ to a high of 10^{-3} $\Omega\,\mathrm{cm}^2$ at 4.2 K. The lowest ρ_c we have obtained is about 8×10^{-5} $\Omega\,\mathrm{cm}^2$ at 4.2 K, which is also the best value reported in the literature[1] for *ex-situ* *c*-axis YBCO/Au junctions. By optimizing fabrication conditions such as ion-milling energy, we were able to consistently fabricate junctions with ρ_c (4.2 K) in this range.

The temperature dependence of the junction resistance exhibits a semiconductorlike behavior; that is, the junction resistance increases with decreasing temperature. For junctions with high interface resistivities, in 10^{-3}-$\Omega\,\mathrm{cm}^2$ range for example, the resistance below 77 K could be 5–7 times that at room temperature. High-interface-quality junctions with ρ_c's in the low 10^{-4}-$\Omega\,\mathrm{cm}^2$ range, on the other hand, are less temperature dependent. Their resistance below 77 K is about 2–3 times that at room temperature. Moreover, high-quality junctions on the same wafer having different junction areas also display more uniform ρ_c's, as demonstrated by good

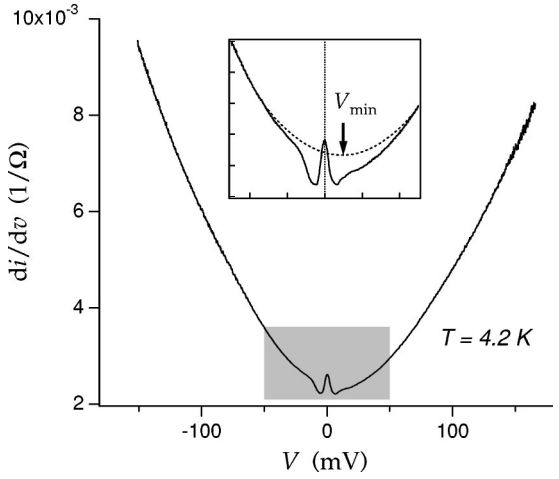

FIG. 1. Conductance vs voltage characteristics of a junction at 4.2 K. The details of the low-bias voltage region (shaded) are shown in the inset.

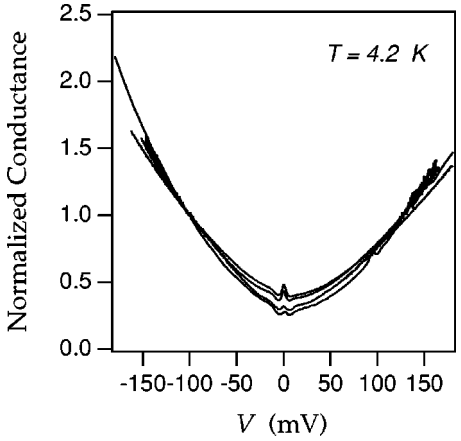

FIG. 2. Normalized conductance vs voltage behavior of four junctions. Each curve is normalized by its conductance value at a bias voltage of -100 mV. The two junctions with higher zero-bias-conductance peaks have smaller values of ρ_c, about 10^{-4} (Ω cm^2) at 4.2 K. The two junctions with lower zero-bias-conductance peaks have larger values of ρ_c(4.2 K): about 10^{-3}(Ω cm^2) and 5×10^{-3}(Ω cm^2), respectively.

resistance-versus-area scaling. Detailed discussions about fabrication and optimization are given in an earlier publication.[1]

III. RESULTS OF JUNCTION CONDUCTANCE MEASUREMENTS

In our system for measuring junction conductance, the dc-current-vs-voltage characteristic is measured simultaneously with the first derivative, di/dv. The latter was measured by superimposing a small-amplitude ac modulation on the dc bias, and detecting the voltage response of the junction using a lock-in amplifier. Data were buffered during acquisition to improve the rate of acquisition while maintaining the desired resolution.

A typical low-temperature conductance-vs-voltage curve for our junctions at 4.2 K is shown in Fig. 1. The inset shows details of the low-bias-voltage range. There are several features that become immediately apparant. First, there is a conductance peak centered at zero bias. Second, except for the conductance peak near zero bias, there is a marked reduction in conductance at bias levels below about 35 mV. This is best seen in the inset of Fig. 1 by comparing the low-bias conductance data with the dashed line, which is an extrapolation from conductance at higher bias. Third, the conductance-vs-voltage behavior is asymmetric: the conductance at forward bias is smaller than its corresponding value at reverse bias. (Forward bias corresponds to the YBCO electrode being positive with respect to the Au electrode.)

There has been considerable controversy surrounding the issue of the zero-bias conductance peak (ZBCP) in YBCO/noble-metal junctions. The general consensus is that this is a result of *d*-wave pairing in YBCO.[2–5] The conductance reduction for a bias below about 30 mV is due to the formation of the superconducting gap in YBCO, which had been extensively studied and well documented.[6] For our present purpose, it suffices to say that both these features are associated with superconducting properties of YBCO. If we were able to suppress the onset of superconductivity in YBCO at low temperatures, then the conductance-vs-voltage characteristic would follow the dashed line in the inset of Fig. 1, showing a conductance minimum at a positive bias, $V_{\min}>0$.

In order to show the systematic behavior of the conductance-vs-voltage characteristics, we plotted normalized conductance curves for four junctions in Fig. 2. Each curve is normalized by its value at -100 mV. This bias voltage is chosen because it is high enough so that the conductance at this voltage is not influenced by the superconducting properties of YBCO. The two junctions with a more pronounced normalized ZBCP feature have larger nominal areas of 64 μm^2. Both have ρ_c values at 4.2 K of about 10^{-4} Ω cm^2. The other two junctions with a weaker normalized ZBCP feature have nominal junction areas of 16 and 4 μm^2. Their ρ_c values at 4.2 K are about 10^{-3} and 5×10^{-3} Ω cm^2, respectively.

Despite the large variations in junction area and specific interface resistivity, the normalized conductance-vs-voltage curves for all the junctions show conductance asymmetry, with a conductance minimum at a nonzero voltage. It follows that we should seek a physical model for this interface system that can explain features of the conductance characteristics. Moreover, the model must be consistent with known material characteristics of the YBCO/Au junction system, such as the existence of a semiconducting/insulating interface layer that acts electrically as a tunneling barrier with low barrier-height.

To our knowledge, there are two types of models of electron tunneling that address the issues of conductance asymmetry and a non-zero-voltage conductance minimum. The first type applies to metal-insulator-metal tunnel junctions. An example is given in the paper by Brinkman, Dynes, and Rowell.[7] These authors studied electron tunneling in aluminum-insulator-metal tunnel junctions (metal=Pb, Sn, or In). They used a trapezoidal potential to model the tunnel

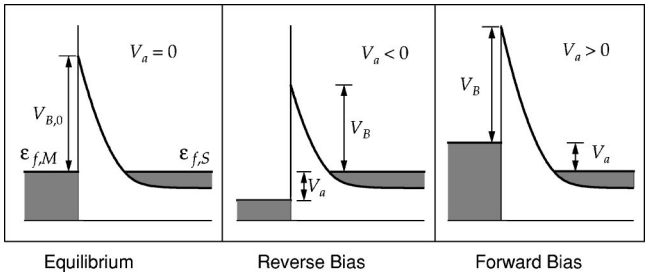

FIG. 3. The Schottky-barrier model for a metal/semiconductor contact. The right-hand side of the interface depicts an *n*-type degenerate semiconductor with Fermi energy $\varepsilon_{f,S}$ and band bending near the interface. The left-hand side is a normal metal with Fermi energy $\varepsilon_{f,M}$. We define forward bias as the semiconductor (or in our case the YBCO superconductor) biased positively with respect to the metal; hence its Fermi energy is lower, as shown in the right panel. The energy profile for a *p*-type semiconductor is just the symmetrical reverse of the *n*-type: the band bends down near the interface, and instead of filled states below $\varepsilon_{f,S}$ in the conduction band, empty states above the Fermi level in the valence band are involved in the tunneling.

barrier. They found that the minimum conductance is not at zero bias unless the barrier is symmetrical and both metal electrodes have the same Fermi energy. The unperturbed barrier height for their system was several electron volts, appropriate for their tunnel barrier, which was aluminum oxide. Such a large value of barrier height is not applicable to our YBCO/Au tunnel junctions, in which the insulating layer behaves more like a semiconductor, and hence the barrier height is likely to be much lower.

The second type of model applies to junctions formed at a metal/semiconductor interface. The model is more commonly known as the Schottky-barrier model. This model also predicts a tunneling-conductance asymmetry, as well as a non-zero-bias conductance minimum. In this model, the relatively small carrier density in the semiconductor plays an important role in determining the tunneling characteristics. It is therefore a more suitable model for our junctions. In Sec. IV, we first introduce the physical motivation for this model and then present the results of a detailed model calculation.

IV. SCHOTTKY-BARRIER MODEL

Figure 3 depicts the basics of the Schottky-barrier model. It shows electron potential profiles across the interface formed between a metal and an *n*-type degenerate semiconductor under various bias conditions.

The left panel shows the system with zero bias potential. On the left-hand side is a metal electrode for which the free-electron model is a good approximation: its energy levels are filled up to the Fermi energy $\varepsilon_{f,M}$. On the right-hand side is a semiconductor (or the *c*-axis surface of the YBCO high-T_c superconductor in our case) with a high dopant concentration such that its Fermi level $\varepsilon_{f,S}$ resides in the conduction band. The two Fermi energies are aligned under equilibrium. Due to the difference in work-functions and surface dipole moment, the semiconductor conduction band ''bends'' up at the interface. The band bending extends over many atomic layers into the semiconductor, forming a potential barrier of height V_{B0} at equilibrium. When the dopant concentration is high, the barrier is very thin and electron tunneling becomes the dominant conduction mechanism at low temperatures.

The middle panel shows the system with reverse bias potential. According to our convention, the YBCO superconductor is biased negatively with respect to the normal metal; hence its Fermi energy is raised with respect to that of the metal in proportion to the applied voltage, V_a. Electrons tunnel predominately from the semiconductor to the metal. The potential barrier seen by these tunneling electrons is lowered from the equilibrium value. Moreover, there is a particular bias voltage, $V_a = V_{min}$, at which the conduction-band edge in the semiconductor aligns with the Fermi level of the metal. This is the voltage at which a conductance minimum is expected to occur.

At forward bias, shown in the right panel, the Fermi level of the metal is raised above that of the semiconductor, and electrons tunnel mostly from the metal into the semiconductor. The potential barrier seen by these electrons, however, remains the same as the equilibrium value. This is because the position of the metal Fermi level with respect to the semiconductor conduction band is ''pinned'' by a high density of surface states. Consequently the tunnel-barrier height remains the same in spite of the increase in (forward) applied voltage. The barrier width is thinner than the equilibrium width, however.

From the above discussion we see that the barrier height seen by tunneling electrons is asymmetric with respect to the polarity of the bias potential, and consequently the tunneling conductance is also asymmetric. Additionally, a conductance minimum is expected to occur at a bias potential equal to the Fermi degeneracy of the semiconductor. For an *n*-type semiconductor, the minimum occurs at a negative bias potential (according to our convention for the bias polarity). For a *p*-type semiconductor it occurs at a positive bias. The fact that we consistently observed a conductance minimum at a positive bias $V_{min} > 0$, is convincing evidence that the *c*-axis surface of YBCO behaves much like a *p*-type, degenerate semiconductor.

It is not surprising that the surface of a YBCO thin film should behave like a semiconductor. Since YBCO in the normal state behaves like a metal with a low carrier density that is close to the limit of a metal-insulator transition, any disorder at the surface will render it semiconducting, even insulating.

There exists an extensive literature on the theory of metal/semiconductor junctions in the context of the Schottky-barrier model. Of particular interest to us is the theory of Conley and Mahan,[8] who calculated the tunneling conductance $\mathrm{d}i/\mathrm{d}v$ for a Schottky-barrier junction. They assume that the semiconductor is *n*-type and degenerately doped. The parameters in their theory are the barrier-height V_{B0} and the Fermi degeneracy $\varepsilon_{f,S}$ of the semiconductor. Modifying their theory slightly to accommodate our situation of a *p*-type semiconductor, we calculate $\mathrm{d}i/\mathrm{d}v$ versus bias-voltage for our junction system, using V_{B0} and $\varepsilon_{f,S}$ as parameters. We find a reasonable agreement with experimental data only

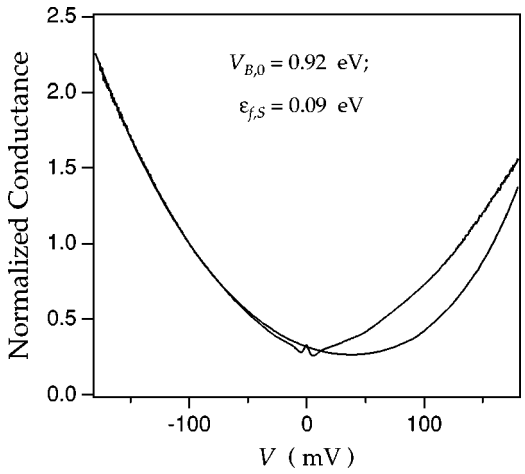

FIG. 4. Comparison of experimental and theoretical conductance vs voltage characteristics. The experimental curve (with a small peak at zero-bias) is obtained at 4.2 K. The model calculation was made assuming $T=0$. Both curves are normalized at a bias voltage of -100 mV.

when the two parameters are varied over rather narrow ranges centered around $V_{B0} \simeq 1$ eV, and $\varepsilon_{f,S} \simeq 0.1$ eV. Figure 4 compares the calculational result with the experimental data. Note that the theoretical curve was calculated using $V_{B0}=0.92$ eV and $\varepsilon_{f,S}=0.09$ eV. Note also that the conductance of both curves is normalized at a bias $V=-100$ mV.

In assessing the quality of the agreement between the theory and experiment, we need to keep in mind that the zero-bias conductance peak in the experimental data is due purely to the superconducting property of one of the electrodes. Since there was no such mechanism built into Conley and Mahan's theory, this peak is not present in the theoretical curve. The agreement for the negative-bias region is quite good. For the positive-bias region, however, the agreement is poor. First, the theory underestimates the magnitude of the normalized conductance by a substantial margin. Second, the theoretical curve has a broad minimum at about 50 mV, while the minimum in the experimental curve occurs at about 20 mV.

Attempts to adjust the two fitting parameters failed to improve the agreement appreciably; instead this often resulted in poorer agreement once the parameters fell outside the narrow ranges mentioned previously. We believe the discrepancy at positive bias is due to the important role of defect-induced localized states at the interface, which was not taken into account in the simple theory of Conley and Mahan. While such defects inevitably exist in any real interface systems, they are particularly prevalent in *c*-axis YBCO junctions, due to its material properties.

Now let us consider how defect-induced localized states would alter our tunneling model. A primary consequency of surface disorder and localized states is ''band tailing''; that is, instead of a well-defined band edge, the conduction band will have a ''tail'' that extends well into the band gap in Fig. 3. Let us also invert the potential profile for the semiconductor so that the filled states in the conduction band become empty states in the valence band—a scenario for a *p*-type degenerate semiconductor. Then at reverse bias, where the semiconductor Fermi level is raised above the metal's Fermi level, the dominant conduction process is electron tunneling from the filled valence states into empty states in the metal. Thus, at reverse bias, the existence of band-tailing has a negligible influence. At forward bias, however, the Fermi level of the metal is raised and electrons tunnel predominantly from the metal into the empty valence states of the semiconductor. Thus, at forward bias band-tailing significantly influences the tunneling process: instead of experiencing diminishing empty states as the valence band-edge is approached (as they would with a well-defined valence band edge), the tunneling electrons encounter a distribution of localized states into which they can still tunnel. Consequently, as the bias potential sweeps through zero and increases in the positive direction, the tunneling conductance reverses the decreasing trend more quickly, resulting in a smaller V_{min} (still positive) than it would have, had there been no localized states. Moreover, as the forward bias potential is further increased, the magnitude of tunneling conductance is enhanced over what it would have been if there were no localized states. Thus, both features of the ''band-tailing'' hypothesis would explain the deviation of the experimental curve from the theoretical curve at positive bias in Fig. 4.

Despite the disagreement between the theoretical and experimental curves at positive bias potential, we believe that the fundamentals of the model remain valid for our junction system. Not only does the model capture the essential qualitative features of the data, it also produces fitting parameters with values that are quite reasonable. For example, we can estimate carrier density near the surface of our *c*-axis YBCO films from the Fermi-energy parameter ε_F. Following Gor'kov and Kopnin[9] we assume a cylindrical Fermi surface for YBCO. Then the energy-momentum spectrum and carrier density are given by

$$\varepsilon = \frac{\hbar^2 k^2}{2m_{ab}} \tag{1}$$

and

$$n = \frac{z k_F^2}{2\pi c_0}, \tag{2}$$

where m_{ab} is the effective mass in the *ab*-plane of YBCO, c_0 is the unit cell length along the *c* axis, and *z* is the number of layers in a unit cell. For YBCO, $c_0=11.7$ Å, and $z=3$. From the review by Gor'kov and Kopnin, we find $m_{ab}=2.6\ m_e$ where m_e is the free-electron mass. Substituting 0.1 eV for the Fermi energy in Eq. (1) we obtain, for the Fermi vector, $k_F \approx 0.26\times 10^8$ cm^{-1}. Using this value, and values for c_0 and *z* we find from Eq. (2) that $n \approx 3\times 10^{21}$ cm^{-3}. This is about one-third the bulk value for single-crystal $YBa_2Cu_3O_7$. It explains why the *c*-axis YBCO thin-film surface would behave more like a semiconducting material.

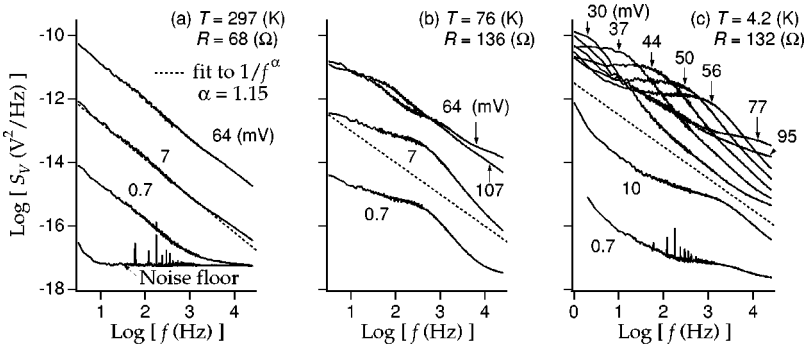

FIG. 5. Noise-power-density spectra of a junction at (a) room temperature, (b) liquid-nitrogen temperature, and (c) liquid-helium temperature. The resistance shown for each temperature is the junction resistance near zero bias. The number associated with each curve is the bias voltage, in units of mV, under which the spectrum was obtained. The room temperature spectra show clear $1/f$ behavior, as demonstrated by the fit. The bias-current values corresponding to each voltage are 0.01, 0.1 and 1 mA. The four spectra at 76 K (bias current $=0.005$, 0.05, 0.5, and 1 mA) do not have a simple $1/f$ dependence. The low-bias spectra display Lorentzian characteristics, while the high-bias spectra resemble more closely a $1/f$ shape, which is represented by the dashed straight line. The spectra at 4.2 K again show a pronounced voltage dependence. From 30 to 77 mV, the noise is dominated by a two-level fluctuator whose corner frequency increases with increasing bias voltage.

V. LOW-FREQUENCY NOISE STUDY

The noise characteristics of YBCO/metal interfaces provide additional evidence of the existence of localized states. Generally, tunnel junctions exhibit excess low-frequency noise with a $1/f$-like power spectrum: $S(f)\propto 1/f$. Studies by Rogers and Buhrman[10] have also shown that small-area superconductor-insulator-superconductor junctions at low temperatures often show a Lorentzian noise spectrum, defined by $S(f)\propto f_c/(f_c^2+f^2)$, where f_c is a characteristic corner frequency. Moreover, they demonstrated that a few such spectra with their corner frequencies appropriately distributed could produce a spectrum that mimics the $1/f$ dependence. Rogers and Buhrman attributed their tunnel junction noise to electron traps in the tunnel barrier. These charge traps can modulate the barrier potential by capturing and subsequently releasing electrons, resulting in tunneling resistance noise. Since interface states appear to play a significant role in tunneling characteristics in our junctions, we expected our junctions to also exhibit excess low-frequency noise, and so we developed a low-frequency noise measurement system[11] to investigate this effect.

Figure 5 displays a junction's noise-power-density spectra, S_v vs f, at (a) room temperature (b) liquid-nitrogen temperature, and (c) liquid-helium temperature. The junction had a nominal width of 8 μm and a room-temperature zero-bias resistance of 68Ω. The room-temperature spectra show a clear $1/f$ frequency dependence. A fit to S_V with the form $1/f^{\alpha}$ yields $\alpha=1.15$, very close to unity. Moreover, S_V is proportional to the square of the bias current I_b: $S_V\propto I_b^2$. This indicates that the noise is due to resistance fluctuation.

At 76 K, the noise spectral shape depends on the bias voltage: for low-bias voltage it has the characteristics of a Lorentzian spectrum. It has very little frequency dependence below the corner frequency f_c, but rolls off rapidly beyond that frequency (as $1/f^2$). As bias voltage increases, the spectra evolves into a $1/f$-like dependence, indicated by the dashed lines in Fig. 5.

At 4.2 K, the noise spectral shape again shows a strong dependence on bias voltage. We see a clear demonstration of the Lorentzian form for voltages between 30 mV and 56 mV, with the corner frequency increasing with bias voltage. At a higher bias voltage (for example the 77 mV and 95 mV curves in Fig. 5) the spectral shape begins to resemble more closely the $1/f$ form (the dashed line), but still with marked deviations. Despite the more varied and complex form of the noise spectra at lower temperatures, the $1/f$ dependence appears to prevail over a wide range of frequency and bias voltage. That is, the curves in Fig. 5(c) may be characterized as displaying an overall $1/f$ ''landscape'' with a few Lorentzian ''bumps.''

Given these observations about the general features exhibited in Fig. 5, we see that a useful way to parametrize our noise data over the range of frequency and bias voltage used in our measurement is to introduce a dimensionless parameter defined by the following equation:

$$\alpha_N=\frac{fS_V}{V^2}=\frac{fS_V}{(I_bR)^2}=\frac{fS_R}{R^2}, \tag{3}$$

where f is frequency, I_b is the bias current, R is the junction resistance at a given bias, and S_R denotes the power spectral density of resistance noise. This normalization procedure was first used by Hooge[12] to compare noise measurement results from a variety of sources on homogeneous semiconductor materials and on inhomogeneous semiconductor structures (such as p-n junctions.) In its original form, Hooge's law (as it has been known since then) reads

$$\frac{S_R}{R^2}=\frac{\alpha}{fN}, \tag{4}$$

where α is a parameter and N is the number of electrons (or charge carriers) in the sample under measurement. The inclusion and the interpretation of N has been a matter of controversy, but was necessary for Hooge to eliminate the large variation in sample size and carrier concentration that he

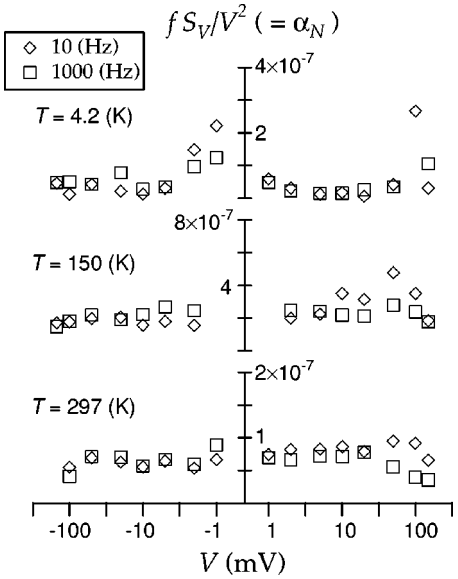

FIG. 6. The normalized noise-power spectral density, fS_V/V^2 ($\equiv\alpha_N$), at 10 Hz (◇) and 1000 Hz (□) plotted vs bias voltage for temperatures of 297 K (lower set of data), 150 K (middle set), and 4.2 K (top set). Note that the data at each temperature are all within a factor of 2, except for a few isolated points such as the one at 100 mV and 4.2 K. The device has a nominal width of 8 μm. Its zero-bias resistances at room temperature and at 4.2 K are 265Ω and 1200Ω, respectively.

encountered. By applying this procedure, Hooge arrive at the empirical conclusion that the parameter α is about 2×10^{-3}, with a small spread. Since neither our sample size nor our carrier density vary greatly, we eliminate the use of N in Hooge's formula. Instead we use a single dimensionless parameter α_N, equivalent to Hooge's α/N, to parameterize the magnitude of the $1/f$ noise component of our junctions.

Figure 6 shows α_N at 10 Hz (◇) and at 1000 Hz (□) of an 8-μm-wide junction at room temperature, 150 K, and 4.2 K, and for bias voltage from −150 to 150 mV. At room temperature, due to the predominantly $1/f$ spectral shape for all the bias voltages, α_N shows no significant dependence on either bias or frequency. Its mean value is about 7×10^{-8}.

At lower temperatures and at certain biases α_N could jump to much greater values, sometimes as much as ten times greater. For example, at 4.2 K and 100 mV, α_N(10 Hz) (the ◇ symbol) was noticeably greater than at other biases; and α_N(1000 Hz), being about 1.7×10^{-6}, was far beyond the axis scale and hence not shown in the figure. All these unusually large α_N's corresponded to noise power spectra that deviated significantly from the simple $1/f$ dependence. Indeed, the noise power spectrum at 4.2 K and 100 mV was a Lorentzian with a corner frequency above 1000 Hz.

Excluding these isolated cases, α_N showed only a weak dependence on bias and frequency in our measurement range, and had a well defined mean value for a given temperature. This mean value is plotted in Fig. 7 for several temperatures.

Fig. 7 has several interesting features. First, the mean

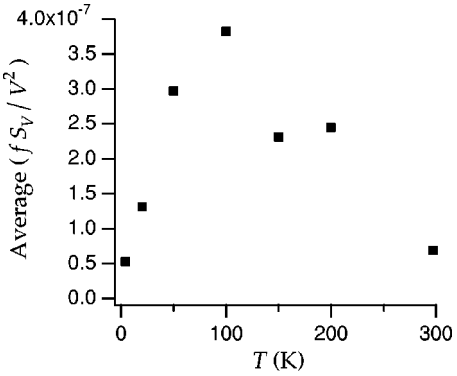

FIG. 7. The temperature dependence of the average of the normalized noise, $fS_V/V^2(=\alpha_N)$, at 10 and 1000 Hz. The average was over the data from one sample, part of which is shown in Fig. 6. The maximum occurred at around 100 K.

value of α_N at 4.2 K was about the same as that at 297 K, despite a nearly five times difference in the junction resistance: 1200Ω at 4.2 K and 265Ω at 297 K. Second, a maximum in α_N occurred at about 100 K. Third, α_N appeared to increase monotonically from 4.2 to 100 K, where it had a maximum of $=4\times10^{-7}$. Below we use this data in a "worst-case scenario" analysis of the noise characteristics of the YBCO/Au interface.

Inverting Eq. (3) we have

$$\frac{S_R}{R^2}=\frac{\alpha_N}{f}. \tag{5}$$

Substituting 4×10^{-7} for α_N and taking the square root of both sides of the above equation we get

$$\frac{\delta R}{R}=\frac{6.3\times10^{-4}}{\sqrt{f}}, \tag{6}$$

in units of $\mathrm{Hz}^{-1/2}$, where δR is the rms value of resistance fluctuation. If, for example, the junction is to be operated at 5 MHz (in a front-end receiver for a low-field magnetic-resonance-imaging system, for instance), Eq. (6) predicts that the normalized resistance noise, $\delta R/R$, will be about 2.8×10^{-7} $\mathrm{Hz}^{-1/2}$. Moreover, assuming that the junction's linear dimension is 100μ m (typical for a wirebond contact,) and that its specific contact resistance is $10^{-3}\Omega$ cm^2, then the junction resistance will be about 10Ω. Thus the expected rms value of the resistance fluctuation, δR, in a unit bandwidth, will be $2.8\times10^{-6}\Omega$.

Although the data in Fig. 7 were taken from one device, the above simple calculation is still instructive. It gives a circuit-engineer an estimate of the magnitude of resistance noise arising from YBCO/Au contacts when they are employed in devices and circuits to be operated in the 4–100-K temperature range.

We do not know any physical mechanisms that may give rise to the pronounced maximum of α_N at 100 K. In our experience, $\delta R/R$ was always larger at 10 and 1000 Hz when the noise power spectrum resembled a Lorentzian than when it was a simple $1/f$. The average of the normalized resistance

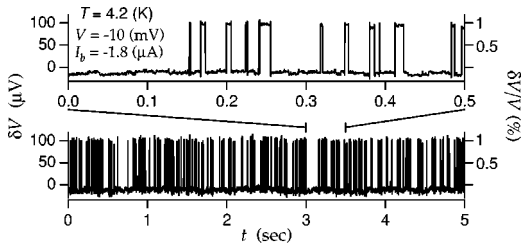

FIG. 8. Voltage-noise time trace of a 4-μm-wide junction at 4.2 K. The upper panel is an expansion of a small section of the lower panel. The two-level random telegraph signal is clearly demonstrated. The small negative value of the lower level was probably due to a dc offset in our preamplifier.

noise α_N had a maximum near 100 K because the Lorentzian-like noise power spectra occurred more often near this temperature. Why it was so we do not know. We now turn to a more detailed analysis of the Lorentzia noise power spectrum.

A Lorentzian spectrum can be modeled by random telegraph signals (RTS) that switch randomly between two well defined levels, each with a mean lifetime of occupancy. Figure 8 shows the time trace of voltage noise for a junction at 4.2 K at a reverse bias voltage of 10 mV with a $=-1.77$ μA bias current. The junction's nominal width is 4 μm, with a zero-bias resistance at 4.2 K of 5300Ω. The lower panel of Fig. 8 displays the time trace over a 5-sec period. The upper panel expands the lower panel and displays a 0.5 sec segment of lower panel. It is clear from the upper panel that what appears to be many ''spikes'' in the lower panel are actually transitions to another (well defined) voltage level that has a much shorter mean lifetime. The lower level is about -10 μV and the upper level about 100 μV. So the transition amplitude, δV, is about 110 μV, which is about 1% of the dc bias voltage.

Figure 9 shows the power spectrum (solid line) of the time trace, part of which is shown in Fig. 8. As expected, the power spectrum is a perfect Lorentzian with a corner frequency of about 100 Hz. The open diamond symbol in Fig. 9 resulted from a calculation based on a formula by Machlup.[13] Machlup calculated the power spectrum of a two-parameter RTS model: a ''one'' state with a mean lifetime of τ_A, and a ''zero'' state with a mean lifetime of τ_B. He found

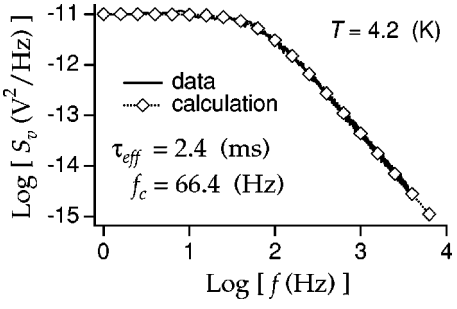

FIG. 9. Noise-power-spectrum data (solid line) and calculational results (open symbol) obtained using a Lorentzian function. The corner frequency f_c of the Lorentzian was derived from an analysis of the time trace shown in Fig. 8. The effective mean lifetime τ_{eff} is related to f_c by Eq. (8a). See the text for details.

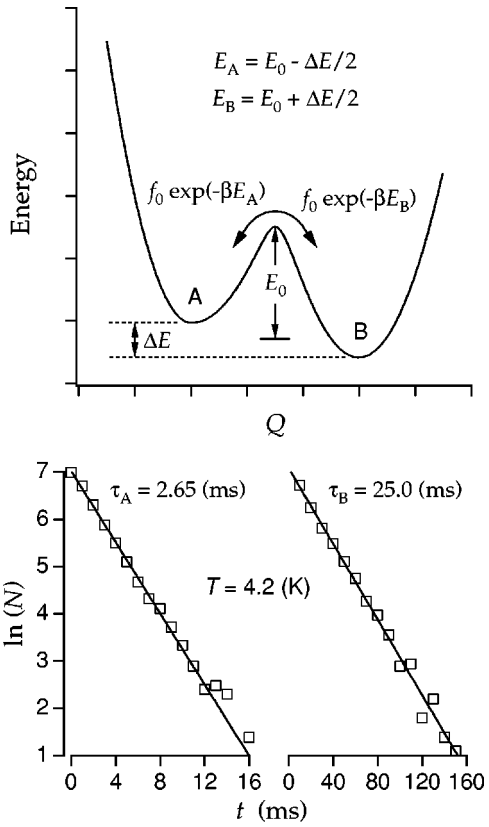

FIG. 10. Upper panel: diagram depicting a two-level system. The system can be characterized by thermal activation energies E_A and E_B for each two states, or by another set of energy parameters ΔE and E_0. Lower panel: histograms of lifetimes of the upper state (A) and the lower state (B) of the time trace shown in Fig. 8. Lines depict a linear fit to the data. The (inverse) of the slopes yield the mean lifetime of each state.

$$S(\omega)=\frac{1}{\pi}\frac{\tau_A\tau_B}{(\tau_A+\tau_B)^2}\frac{\dfrac{1}{\tau_A}+\dfrac{1}{\tau_B}}{\left(\dfrac{1}{\tau_A}+\dfrac{1}{\tau_B}\right)^2+\omega^2}. \tag{7}$$

The physical motivation for Machlup's RTS model is depicted in the upper panel of Fig. 10. The diagram shows the energy of a single two-state system as a function of the configuration coordinate, Q. Given that the system is initially in one of the two states (labeled A and B) there is a certain probability that it will be found in the other state at a given later time. The rate of transition, or the inverse of the mean lifetime, has the usual Arrhenius form $1/\tau_{A,B}=2\pi f_0\exp(-\beta E_{A,B})$, where $E_{A,B}$ are the thermal activation energies for states A and B respectively, $\beta=(k_BT)^{-1}$, and k_B is the Boltzmann constant. If the junction resistance depends on which state the two-level system occupies, then the system will exhibit resistance fluctuations as it switches between the two states.

Machlup's formula [Eq. (7)] results in a corner frequency $\omega_c=2\pi f_c$ that is given by the sum of the two transition rates between the two states:

$$f_c = \frac{1}{2\pi}\left(\frac{1}{\tau_A}+\frac{1}{\tau_B}\right) = \frac{1}{2\pi\tau_{eff}} \tag{8a}$$

$$= f_0[\exp(-\beta E_A)+\exp(-\beta E_B)]. \tag{8b}$$

Using the parameter f_c and changing to frequency notation ($f=\omega/2\pi$, allowing only positive frequencies), we can rewrite Eq. (7) as a mean-square-voltage noise per unit bandwidth, $S_V(f)$:

$$S_V(f) = \langle(\delta V)^2\rangle \frac{4\tau_A^2\tau_B^2}{(\tau_A+\tau_B)^3}\frac{1}{1+(f/f_c)^2}. \tag{9}$$

Note that Eq. (9) has units of (V^2/Hz) since we have replaced the unit step size of Eq. (7) with the mean square of voltage noise $\langle(\delta V)^2\rangle$. In rewriting Eq. (7) to Eq. (9) we also introduced a prefactor of 4π: 2π due to the change in variable $f=\omega/2\pi$, and another factor of 2 resulting from a folding of the frequency range from $-\infty<\omega<\infty$ to $0<f<\infty$ (only positive frequencies are permitted).

Equations (8) and (9) enable us to calculate the noise-power spectrum if the parameters δV, τ_A, and τ_B are known. By analyzing hundreds of time-trace records such as shown in Fig. 8, we obtained statistically meaningful time distributions for the two states. The lower panel of Fig. 10 shows histograms of lifetimes for state A (the upper level) and state B (the lower level). Since these are semi-log plots, a linear dependence corresponds to an exponential time correlation function, $\exp(-t/\tau)$. The inverse of the linear slopes gives mean lifetimes $\tau_A=2.65$ ms and $\tau_B=25.0$ ms, for the upper and lower levels respectively. Substituting these values in Eq. (8a) we find that the corner frequency is $f_c=66.4$ Hz. Also, from Fig. 8 we see that $\delta V=110\times10^{-6}$ V. Substituting these numbers into Eq. (9) we calculate the function $S_V(f)$ and plot the result in Fig. 9 (the $\diamond$ symbol). The agreement with the experimental data is excellent, with no adjustable parameters.

A Lorentzian spectrum similar to that shown in Fig. 9 was reported by Myers *et al.*[14] in $YBa_2Cu_3O_{7-\delta}$/$CaRuO_3$/$YBa_2Cu_3O_{7-\delta}$ Josephson junctions. The Lorentzian spectrum therefore appears to be a rather general feature of YBCO interfaces.

Rogers and Buhrman[10] identified the origin of the two-level fluctuations with electron trap-and-release events at defect states in the tunnel barrier. In our system the most probable candidates for such defect states are the surface and interface states of YBCO. We have shown indirect evidence for these states from our transport measurements. Our low-frequency noise data provide more direct evidence. Further experiments are needed to probe the energy distribution of these states.

VI. CONCLUSIONS

Low-temperature interface transport in our *c*-axis YBCO/Au junctions can be adequately described by a model based on Schottky-barrier tunneling. The theory models the *c*-axis YBCO interface as a *p*-type degenerate semiconductor, with a Fermi energy of 0.1 eV. Two main characteristics of this model are conductance asymmetry and a conductance minimum at a finite bias voltage. In our convention for bias polarity, the conductance at forward bias is smaller than that at the corresponding reverse bias, and there is a forward bias voltage, $V_{min}>0$, at which the conductance minimum occurs. Both of these features are consistently observed in our extensive data sets.

We can calculate the tunneling conductance using the theoretical model and two parameters: the barrier height ($\approx$1.0 eV) and the Fermi energy of YBCO ($\approx$0.1 eV). The agreement with experiment is very good for the reverse bias direction. The discrepancy for the forward bias direction can be explained qualitatively by the dominant role of localized electron states at the YBCO interface, which our simple theory ignored completely. Our results clearly indicate the need to incorporate the role of localized states into the theory. We have not attempted to do that since our current knowledge about localized states at the YBCO interface is far from adequate. However, the success of our model in predicting qualitatively the general conductance features points the way toward a more comprehensive understanding of interface transport of high-T_c superconductor/noble-metal systems.

Systematic measurements of low-frequency noise in our junctions show that $1/f$-like resistance noise dominates *c*-axis YBCO/Au junctions at room temperature for bias voltage up to 150 mV and frequencies up to 100 kHz. Not only does the noise still exist at liquid-helium temperature, its magnitude does not vary by more than a factor of about ten over the entire temperature range. Due to the strong presence of $1/f$-like noise over a large range of temperature, bias voltage, and frequency, Hooge's formula can be used to adequately parameterize the overall $1/f$ noise magnitude of our junctions. Consequently we obtain a general number, expressed in Eq. (6), for normalized resistance noise. The significance of this number is that it is applicable for the range of temperature, bias voltage, and frequency that are of particular interest to high-T_c electronics applications. We also demonstrated how these results can be applied to address noise issues in high-T_c electronics.

At low temperatures and for certain bias voltages, our junction noise appears to be also dominated by a particularly strong two-level fluctuator, which can significantly alter the above mentioned $1/f$-like dependence. Unlike the case of niobium-oxide barrier tunnel junctions, the *c*-axis YBCO/Au junctions need not be small in order for a single, two level fluctuator to dominate the noise in a limited bandwidth. Further study of these two level fluctuators, in particular their energy distribution, will likely yield information essential for a better quantitative description of this feature of junction-transport behavior.

ACKNOWLEDGMENTS

A contribution of NIST, an agency of the U.S. government. We gratefully acknowledge the support of the Department of Energy Office of Basic Energy Sciences under Grant No. DE-IA03-94ER14420.

[1] Y. Xu, J.W. Ekin, C.C. Clickner, and R.L. Fiske, in *Advances in Cryogenic Engineering Materials*, edited by U.B. Balachandran *et al.* (Plenum Press, New York, 1998), Vol. 44, Part B, pp. 381–388.
[2] C.-R. Hu, Phys. Rev. Lett. **72**, 1526 (1994).
[3] J.W. Ekin *et al.*, Phys. Rev. B **56**, 13 746 (1997).
[4] M. Covington *et al.*, Phys. Rev. Lett. **79**, 277 (1997).
[5] M. Fogelström, D. Rainer, and J.A. Sauls, Phys. Rev. Lett. **79**, 281 (1997).
[6] J.M. Valles, Jr. *et al.*, Phys. Rev. B **44**, 11 986 (1991).
[7] W.F. Brinkman, R.C. Dynes, and J.M. Rowell, J. Appl. Phys. **41**, 1915 (1970).
[8] J.W. Conley and G.D. Mahan, Phys. Rev. **161**, 681 (1967).
[9] L.P. Gor'kov and N.B. Kopnin, Sov. Phys. Usp. **31**, 850 (1988).
[10] C.T. Rogers and R.A. Buhrman, Phys. Rev. Lett. **53**, 1272 (1984).
[11] Y. Xu, J.W. Ekin, and C.C. Clickner, in *Proceedings of the 1998 Applied Superconductivity Conference*, Palm Springs, California, 1998.
[12] F.N. Hooge, Phys. Lett. **29A**, 139 (1969).
[13] S. Machlup, J. Appl. Phys. **25**, 341 (1954).
[14] K.E. Myers, K. Char, M.S. Colclough, and T.H. Geballe, Appl. Phys. Lett. **64**, 788 (1994).